IJSES
International Journal of Scientific Engineering and Science
Volume 10, Issue 7, pp. 60-65, July 2026.
ISSN (Online): 2456-7361

Monthly Forest Fire Risk Mapping for U Minh Ha National Park Using Landsat and GIS

Ha Thanh Van, Vu Khanh Tuong Van
Ho Chi Minh University of Natural Resources and Environment, Viet Nam

***Abstract*— *Peatland Melaleuca forests in the lower Mekong Delta are highly vulnerable to dry-season fires, but operational fire-risk maps for lowland peat forests remain limited at monthly and management-unit scales. This study developed monthly forest fire-risk maps for U Minh Ha National Park, Ca Mau Province, Vietnam, using Landsat 8 and Landsat 9 imagery acquired from January to April 2025, ancillary forest-status maps, roads, canals, inundation data, meteorological information, and compartment boundaries. Five satellite-derived indicators, including NDVI, EVI, NDWI, MSI, and land surface temperature, were standardized together with forest cover, distance to roads, distance to canals, and inundation condition. The Analytical Hierarchy Process and a Fire Risk Index were used to integrate the nine predictors in a GIS weighted-overlay framework. Results show a strong monthly shift in fire danger. The combined high and very high risk area reached 3,371.43 ha in January, peaked at 4,402.77 ha in February, declined to 2,332.67 ha in March, and reached 1,444.56 ha in April. Sub-compartments 59, 61, 70, 73, 75, and 76 repeatedly appeared as priority zones. The proposed approach provides an interpretable and low-cost basis for dry-season patrol planning, canal-water regulation, and early-warning support in peatland national parks.*

***Keywords*— *AHP, forest fire risk, GIS, Landsat 8 and 9, U Minh Ha National Park.*

I. Introduction

Forest fire is an increasingly important natural-hazard and land-management problem because fire danger is shaped by climate variability, fuel condition, water availability, and human ignition pressure. Global analyses have shown that climate-induced fire-weather conditions have intensified in many regions, increasing the need for spatially explicit and operational warning tools [1]. In tropical peatlands, the problem is more complex than in mineral-soil forests because a surface fire can develop into persistent smoldering combustion, cause long-term carbon emissions, and continue even when flame is not evident at the surface [2]–[4].

Remote sensing and geographic information systems have long been used to translate these drivers into spatial fire-hazard or fire-risk maps. Early work demonstrated that satellite data and GIS layers could be combined to map forest fire hazard across heterogeneous landscapes [5]. More recent studies have advanced this approach by integrating vegetation indices, thermal variables, terrain, accessibility, and human-related factors in multi-criteria or machine-learning frameworks [6], [7]. Landsat imagery is particularly useful for protected-area management because its 30 m multispectral resolution is adequate for compartment-level mapping while its thermal band can support land surface temperature estimation [8].

Several Vietnamese studies provide a relevant foundation. In Cat Ba National Park, a GIS-based kernel logistic regression model was developed to map tropical forest fire susceptibility [9]. In Son La Province, Landsat-derived layers, expert judgement, the Analytic Hierarchy Process, and multi-criteria analysis were used to build provincial fire-risk maps [10]. Later work in northwestern Vietnam coupled AHP and MCA/GIS for risk mapping and early warning [11], while MaxEnt and machine-learning models have been used for regional fire occurrence and fire-risk prediction in northwestern Vietnam and Nghe An Province [12], [13]. These studies confirm the value of geospatial methods but most were designed for mountainous or upland forest systems where slope, elevation, aspect, and population gradients are major controls.

U Minh Ha National Park is different. It is a lowland peatland Melaleuca ecosystem in Ca Mau Province where relief is nearly flat, the fire season is closely linked to dry-season water deficit, canal-water regulation, peat moisture, and human access along roads and canals. Research in nearby U Minh Thuong shows that peat thickness and inundation regime influence Melaleuca regeneration after fire and that year-round water retention can reduce fire danger but may also affect biodiversity [14]. Therefore, a simple transfer of upland fire-risk models to U Minh Ha may produce misleading priorities if hydrological controls and management compartments are not incorporated.

The research gap addressed in this paper is the lack of a monthly, compartment-oriented fire-risk assessment for a Vietnamese lowland peatland national park using medium-resolution satellite data and practical GIS layers. The contributions are threefold: (i) to integrate spectral, thermal, forest-status, hydrological, inundation, and accessibility variables into an interpretable Fire Risk Index; (ii) to map fire-risk classes for each month of the 2025 dry season; and (iii) to identify priority sub-compartments for patrol, water regulation, and prevention planning in U Minh Ha National Park.

II. Materials and Methods

A. Study Area

U Minh Ha National Park is located in Ca Mau Province, southern Vietnam, within approximately 9 degrees 12 minutes 30 seconds to 9 degrees 17 minutes 41 seconds North and 104 degrees 54 minutes 01 seconds to 104 degrees 59 minutes 16 seconds East. The park covers about 8,506.18 ha in the management dataset used in this study and includes sub-compartments distributed across former U Minh and Tran Van Thoi districts. The dominant forest type is Melaleuca on acid sulfate and peat soils, with a dense canal and dike network used

Volume 10, Issue 7, pp. 60-65, July 2026. ISSN (Online): 2456-7361

for water retention, transport, and fire prevention. The climate is tropical monsoon with a pronounced dry season from January to April, which coincides with reduced surface water, higher evaporation, and greater fire danger.

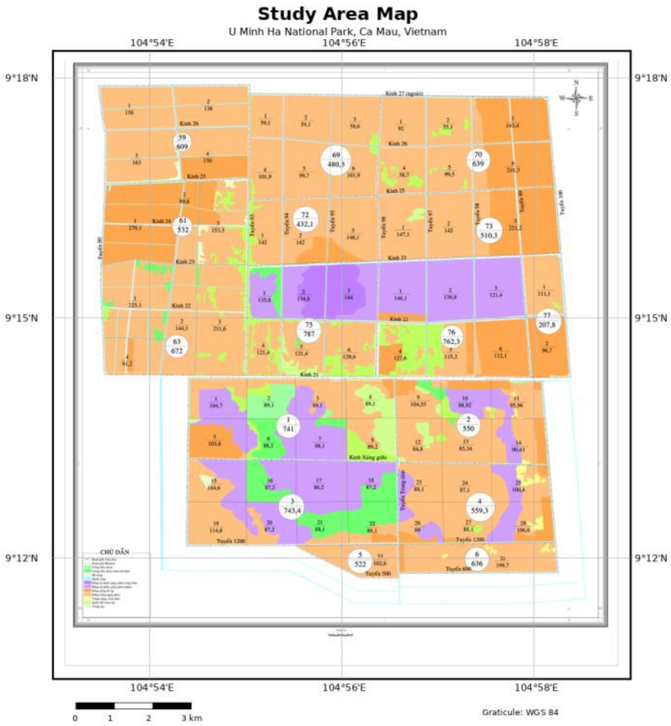

Fig. 1. Study area map of U Minh Ha National Park. The map was standardized with a map frame, graticule, north arrow, scale bar, and legend.

B. Data Sources and Pre-Processing

The analysis used four Landsat scenes acquired during the 2025 dry season and ancillary GIS layers including the national park boundary, sub-compartment boundaries, forest-status maps, road network, canal and river network, inundation condition, meteorological records, and hydrological observations. Landsat scenes were selected based on cloud availability and their temporal representativeness for January, February, March, and April 2025. All spatial datasets were projected to a common coordinate system, clipped to the park boundary, and resampled or rasterized to a 30 m grid.

TABLE I. Landsat 8 and 9 OLI/TIRS scenes used in the study.

No.	Scene ID	Date	Cloud cover (%)	Path/row
1	LC91260542025002LGN00	02 Jan 2025	18.14	126/054
2	LC81260532025058LGN00	27 Feb 2025	11.19	126/053
3	LC91260532025082LGN00	23 Mar 2025	10.64	126/053
4	LC91250542025107LGN00	17 Apr 2025	18.52	125/054

Radiometric conversion and atmospheric correction followed standard Landsat processing principles. Digital numbers were converted to top-of-atmosphere radiance and reflectance using metadata coefficients; atmospheric haze effects were reduced using dark-object subtraction when Level-2 surface reflectance was not directly used. Cloud-affected pixels were visually checked and removed where necessary. The spectral indices were computed from the corrected blue, red, near-infrared, and shortwave-infrared bands. Landsat thermal information was converted to land surface temperature using radiance, brightness temperature, and emissivity correction procedures consistent with established Landsat thermal retrieval studies [8], [15], [16].

C. Fire-Risk Predictors

Nine predictors were used because they represent the three operational components of fire risk in the park: fuel amount and fuel condition, moisture and heat stress, and accessibility or water availability for ignition and suppression. Vegetation greenness was represented by NDVI and EVI, vegetation water condition by NDWI and MSI, heat condition by LST, fuel presence by forest status, human access by distance to roads, suppression water access by distance to canals, and peatland dryness by inundation condition.

$$\text{NDVI} = (\text{NIR} - \text{Red}) / (\text{NIR} + \text{Red}) \quad (1)$$

$$\text{EVI} = 2.5 \times (\text{NIR} - \text{Red}) / (\text{NIR} + 6 \times \text{Red} - 7.5 \times \text{Blue} + 1) \quad (2)$$

$$\text{NDWI} = (\text{NIR} - \text{SWIR}) / (\text{NIR} + \text{SWIR}) \quad (3)$$

$$\text{MSI} = \text{SWIR} / \text{NIR} \quad (4)$$

NDVI is widely used to estimate vegetation vigor and photosynthetically active biomass [17]. EVI improves vegetation monitoring in dense-canopy conditions by reducing atmospheric and soil-background effects [18]. NDWI and MSI capture leaf and canopy water condition because shortwave-infrared reflectance responds to water absorption in vegetation [19], [20]. In this study, higher NDVI, EVI, MSI, LST, forest presence, and proximity to roads increased risk scores, while higher NDWI, proximity to canals, and inundated conditions reduced risk scores.

TABLE II. Reclassification logic used for fire-risk scoring.

Predictor	Observed or classified range	Risk direction
LST	19.3 to 24.8 C	higher value, higher risk
NDVI	0.03 to 0.57	higher value, higher risk
NDWI	-0.14 to 0.39	lower value, higher risk
MSI	0.40 to 1.40	higher value, higher risk
EVI	0.047 to 1.11	higher value, higher risk
Forest status	vegetation or non-vegetation	vegetation, higher risk
Distance to road	200 m intervals	nearer road, higher risk
Distance to canal	150 m intervals	farther canal, higher risk
Inundation	inundated to dry	drier surface, higher risk

TABLE III. AHP weights of factors used in the Fire Risk Index.

Factor	AHP weight
NDVI	0.284
Inundation condition	0.130
Distance to canals and waterways	0.118
MSI	0.090
LST	0.074
NDWI	0.074
EVI	0.067
Forest status	0.050
Distance to roads	0.040

D. Weighting and Fire Risk Index

The Analytic Hierarchy Process was used to determine the relative importance of fire-risk factors based on expert judgement, local fire-prevention knowledge, and evidence from previous GIS-based fire-risk mapping studies [6], [10], [11], [21], [22]. The resulting weights emphasize vegetation status and peatland water condition, which are more relevant in U Minh Ha than topographic slope and aspect. Slope and aspect

International Journal of Scientific Engineering and Science
Volume 10, Issue 7, pp. 60-65, July 2026. ISSN (Online): 2456-7361

were excluded because the park is a nearly flat lowland system and their influence was considered negligible.

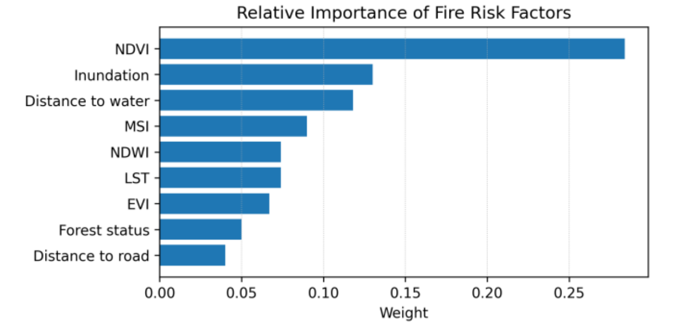

Fig. 2. Relative importance of fire-risk factors used in the weighted overlay.

For each month, the standardized predictor layers were overlaid in GIS using the Fire Risk Index shown in (5). The displayed weights are rounded values; full-precision values were retained during GIS calculation to preserve the AHP priority structure.

FRI_i = sum from j=1 to n of W_j x X_ij (5)

where FRI_i is the fire-risk score at pixel i, W_j is the weight of factor j, and X_ij is the standardized class score of factor j at pixel i. The continuous FRI output was reclassified into five classes corresponding to the Vietnamese forest-fire warning structure: Class I, low; Class II, moderate; Class III, high; Class IV, dangerous; and Class V, extremely dangerous. The final maps were summarized by sub-compartment for management use.

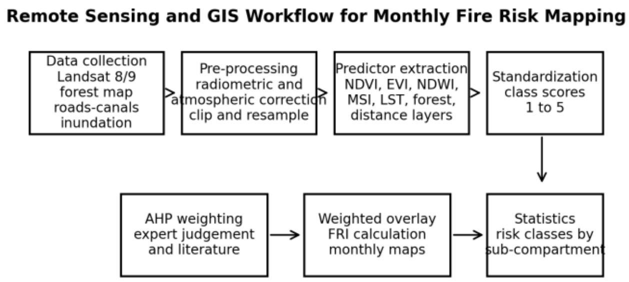

Fig. 3. Workflow used to generate monthly forest fire-risk maps.

III. Results

A. Dry-Season Predictor Patterns

The satellite-derived variables showed clear spatial and monthly differentiation across the park. LST ranged from 19.4 to 24.9 C, with the highest upper value occurring in February. NDVI varied from 0.03 to 0.58, indicating a heterogeneous mixture of dense Melaleuca cover, seasonal wetlands, and lower-cover areas. NDWI ranged approximately from -0.10 to 0.40, while MSI ranged from 0.40 to 1.30, confirming that dry-season moisture stress was spatially uneven. EVI ranged from 0.04 to 1.11 and reinforced the spatial pattern of vegetation concentration and canopy condition.

Vegetation-covered area was lowest in January and highest in March. However, higher vegetation area alone did not fully determine fire danger. The February map produced the largest high-risk footprint because vegetation availability coincided with higher LST, lower moisture conditions in several compartments, and areas farther from accessible water sources.

TABLE IV. Vegetation and non-vegetation areas in the dry season of 2025.

Month	Vegetation area (ha)	Non-vegetation area (ha)
January	6,567.70	1,999.50
February	7,042.80	1,524.40
March	7,234.70	1,332.50
April	6,710.50	1,856.70

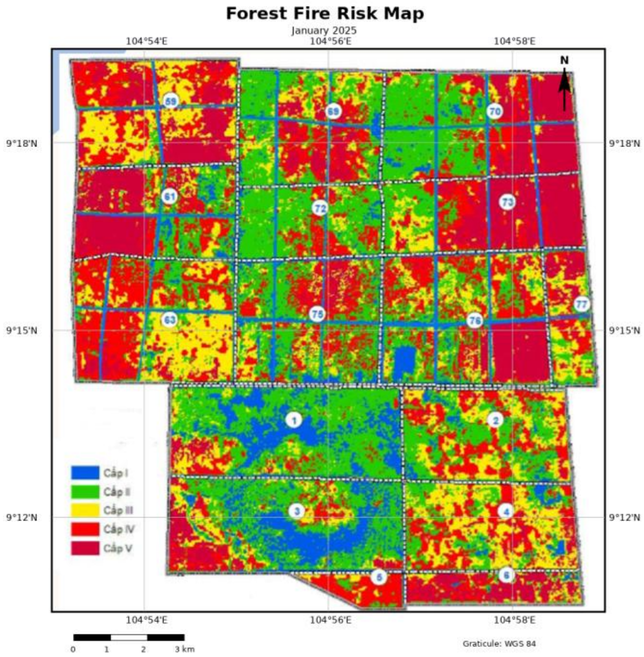

Fig. 4. Forest fire-risk map for January 2025. The map layout includes thematic content, frame, graticule, north arrow, and scale bar.

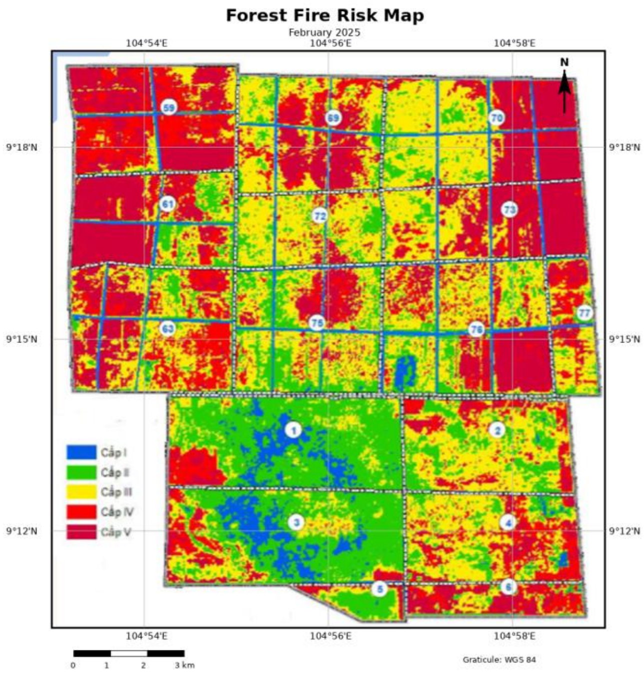

Fig. 5. Forest fire-risk map for February 2025. The map layout includes thematic content, frame, graticule, north arrow, and scale bar.

IJSES
International Journal of Scientific Engineering and Science
Volume 10, Issue 7, pp. 60-65, July 2026.
ISSN (Online): 2456-7361

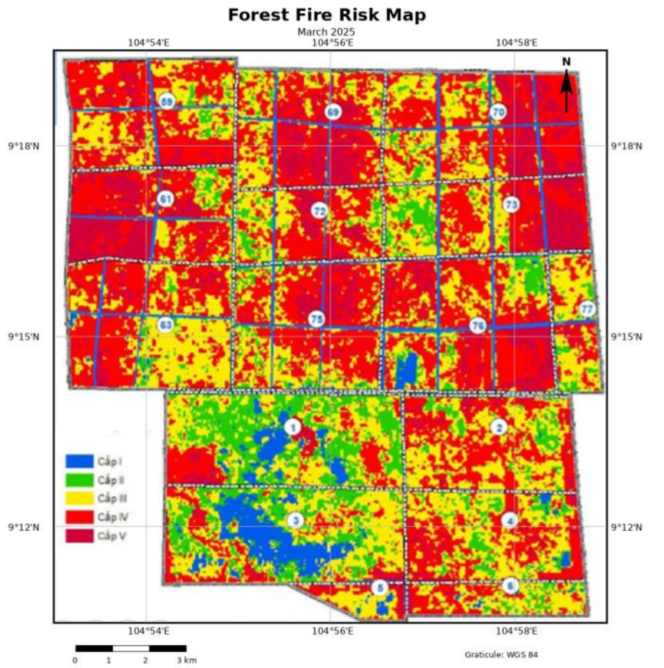

Fig. 6. Forest fire-risk map for March 2025. The map layout includes thematic content, frame, graticule, north arrow, and scale bar.

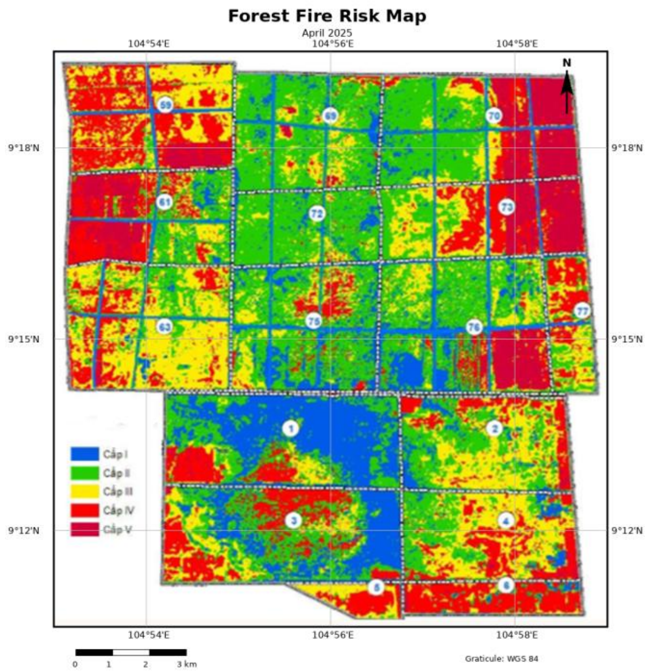

Fig. 7. Forest fire-risk map for April 2025. The map layout includes thematic content, frame, graticule, north arrow, and scale bar.

B. Monthly Forest Fire-Risk Maps

The monthly fire-risk maps reveal a dynamic spatial pattern. In January, Class V risk was extensive in sub-compartments 59, 61, 70, 73, and 76. In February, risk intensified and the combined Class IV and Class V area became the largest of the season, especially in sub-compartments 61, 69, 70, 75, and 76. By March, the area of Class IV and Class V decreased substantially, although sub-compartments 59, 61, 70, and 73 remained important. In April, Class III became the dominant class and Class V was limited, but sub-compartments 59, 61, 70, and 73 still required attention because they retained considerable Class IV risk.

TABLE V. Monthly distribution of fire-risk classes in U Minh Ha National Park.

Month	I	II	III	IV	V	IV+V
January	713.24	2,946.30	1,475.20	1,812.72	1,558.71	3,371.43
February	297.01	947.59	2,862.98	3,232.93	1,169.84	4,402.77
March	1,188.86	3,127.65	1,870.36	1,630.97	701.70	2,332.67
April	460.13	2,784.24	3,817.53	1,048.34	396.22	1,444.56

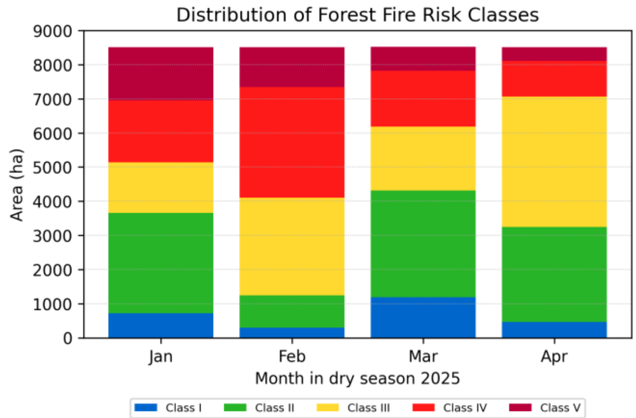

Fig. 8. Area distribution of fire-risk classes from January to April 2025.

TABLE VI. Priority sub-compartments based on the combined Class IV and Class V area.

Month	Priority sub-compartments	Class IV+V area (ha)
January	73, 59, 76, 70, 63	357.25, 356.15, 347.46, 337.07, 336.38
February	76, 70, 61, 69, 75	494.06, 477.73, 398.30, 396.47, 392.23
March	59, 70, 73, 61, 3	339.18, 280.76, 280.22, 265.28, 184.00
April	59, 61, 70, 73, 3	218.67, 195.14, 143.27, 139.38, 118.78

C. Interpretation at Management-Unit Scale

The spatial statistics indicate that fire prevention should not be organized uniformly across the park. February requires the strongest readiness because more than half of the park was classified as Class IV or Class V. Sub-compartment 76 had the largest combined Class IV and Class V area in February, followed by 70, 61, 69, and 75. In January, several compartments had similar high-risk extents, suggesting the need for simultaneous patrols and early water-level checks. In March and April, risk did not disappear; instead, it contracted into fewer recurring compartments, especially 59, 61, 70, and 73. These locations should remain under routine monitoring even after the seasonal peak.

IV. Discussion

The results support the view that fire risk in U Minh Ha is controlled by the interaction of fuel availability, heat stress, and hydrological condition. NDVI received the highest AHP weight because dense Melaleuca vegetation provides fuel continuity. However, the February peak shows that vegetation amount alone is not sufficient to explain fire danger. The coincidence of high LST, moisture stress, reduced inundation, and distance from water created a larger high-risk area than in March, when vegetation cover was higher but the high-risk area had already decreased.

The importance of hydrology is consistent with peatland fire science. Peat fires can burn underground and persist longer than ordinary surface fires, while lower water tables increase the probability of smoldering combustion and carbon loss [2]–[4]. This supports the inclusion of inundation and distance to canals as core variables. For U Minh Ha, maintaining adequate water in the canal system during the dry season is not only a suppression measure but also a risk-prevention measure that keeps peat and surface litter wetter.

Compared with Vietnamese studies in Cat Ba, Son La, northwestern Vietnam, and Nghe An, the proposed model is intentionally simpler and more management-oriented [9]–[13]. Those studies were conducted largely in upland or mixed landscapes where topography, elevation, aspect, and broader socio-economic gradients strongly influence risk. In contrast, U Minh Ha is a low-relief, dike-enclosed peatland. Excluding slope and aspect is therefore methodologically reasonable, while emphasizing inundation, canal distance, and Melaleuca fuel is more consistent with local fire mechanisms.

The approach also aligns with international GIS-based fire-risk mapping studies that use AHP, weighted overlay, and spectral indicators to create interpretable maps for land managers [5]–[7], [21], [22]. The added value here is the monthly dry-season perspective. Annual or static maps can identify generally hazardous places, but monthly maps provide a better basis for deciding when to increase patrol frequency, when to inspect water-control structures, and where to deploy field teams.

Several limitations should be considered. First, the model produces relative risk zones rather than active-fire detections or ignition probabilities validated by 2025 fire points. Second, cloud cover, mixed pixels, and the 30 m Landsat resolution can obscure narrow canals, small openings, and local fuel breaks. Third, the AHP weights are expert-based and should be recalibrated when field fuel-moisture observations, water-table measurements, and more recent fire-occurrence data become available. Future work should integrate Sentinel-2, Sentinel-1 soil-moisture proxies, automatic weather stations, water-level sensors, and machine-learning validation to support near-real-time fire warning.

V. CONCLUSION

This study demonstrates that medium-resolution Landsat data, local GIS layers, and an interpretable weighted-overlay model can be converted into practical monthly fire-risk information for a lowland peatland national park. For U Minh Ha, the most useful output is not only a map of where fire danger is high but also a month-by-month list of compartments where prevention resources should be concentrated.

The findings indicate that peatland fire management should combine remote-sensing surveillance with field-based water regulation. The recurring high-risk compartments identified in this study should be prioritized for patrol scheduling, inspection of canals and sluices, control of human access, and placement of warning signs and observation points during the dry season.

The method can be replicated in other Melaleuca and peatland protected areas in the Mekong Delta after local calibration. Its main advantage is operational transparency: every input layer has a clear management meaning, and the final risk classes can be updated when new satellite scenes, water-level records, or field observations become available.

ACKNOWLEDGMENT

The authors acknowledge the availability of Landsat data and the local forest-management datasets used to support the GIS analysis. Author names, affiliations, and funding information should be completed before submission.

REFERENCES

[1] W. M. Jolly, M. A. Cochrane, P. H. Freeborn, Z. A. Holden, T. J. Brown, G. J. Williamson, and D. M. J. S. Bowman, “Climate-induced variations in global wildfire danger from 1979 to 2013,” Nature Communications, vol. 6, article 7537, 2015, doi: 10.1038/ncomms8537.

[2] S. E. Page, F. Siegert, J. O. Rieley, H.-D. V. Boehm, A. Jaya, and S. Limin, “The amount of carbon released from peat and forest fires in Indonesia during 1997,” Nature, vol. 420, pp. 61-65, 2002, doi: 10.1038/nature01131.

[3] M. R. Turetsky, B. Benscoter, S. Page, G. Rein, G. R. van der Werf, and A. Watts, “Global vulnerability of peatlands to fire and carbon loss,” Nature Geoscience, vol. 8, pp. 11-14, 2015, doi: 10.1038/ngeo2325.

[4] A. Sirin, I. Medvedeva, A. Maslov, D. Vozbrannaya, and D. Makarov, “Remote sensing mapping of peat-fire-burnt areas: identification among other wildfires,” Remote Sensing, vol. 14, no. 1, article 194, 2022, doi: 10.3390/rs14010194.

[5] E. Chuvieco and R. G. Congalton, “Application of remote sensing and geographic information systems to forest fire hazard mapping,” Remote Sensing of Environment, vol. 29, no. 2, pp. 147-159, 1989, doi: 10.1016/0034-4257(89)90023-0.

[6] F. Sivrikaya and O. Kucuk, “Modeling forest fire risk based on GIS-based analytical hierarchy process and statistical analysis in Mediterranean region,” Ecological Informatics, vol. 68, article 101537, 2022, doi: 10.1016/j.ecoinf.2021.101537.

[7] F. Sivrikaya, A. Gunlu, O. Kucuk, and O. Urker, “Forest fire risk mapping with Landsat 8 OLI images: evaluation of the potential use of vegetation indices,” Ecological Informatics, vol. 79, article 102461, 2024, doi: 10.1016/j.ecoinf.2024.102461.

[8] J. C. Jimenez-Munoz, J. A. Sobrino, D. Skokovic, C. Mattar, and J. Cristobal, “Land surface temperature retrieval methods from Landsat-8 thermal infrared sensor data,” IEEE Geoscience and Remote Sensing Letters, vol. 11, no. 10, pp. 1840-1843, 2014, doi: 10.1109/LGRS.2014.2312032.

[9] D. Tien Bui, K.-T. T. Le, V. C. Nguyen, H. D. Le, and I. Revhaug, “Tropical forest fire susceptibility mapping at the Cat Ba National Park area, Hai Phong City, Vietnam, using GIS-based kernel logistic regression,” Remote Sensing, vol. 8, no. 4, article 347, 2016, doi: 10.3390/rs8040347.

[10] N. N. Thanh, D. N. B. Toan, and P. X. Canh, “Remote sensing and GIS application to establish a forest fire risk map for planning of forest fire prevention and mitigation in Son La Province, Vietnam,” VNU Journal of Science: Earth and Environmental Sciences, vol. 33, no. 3, 2017, doi: 10.25073/2588-1094/vnuees.4088.

[11] T. V. Hoang, T. Y. Chou, Y. M. Fang, N. T. Nguyen, Q. H. Nguyen, P. X. Canh, D. N. B. Toan, X. L. Nguyen, and M. E. Meadows, “Mapping forest fire risk and development of early warning system for NW Vietnam using AHP and MCA/GIS methods,” Applied Sciences, vol. 10, no. 12, article 4348, 2020, doi: 10.3390/app10124348.

[12] T. T. Pham, T. Chu, and B. Q. Tran, “Modelling spatial patterns of forest fire occurrence in the Northwestern region of Vietnam,” Vietnam Journal of Earth Sciences, 2024, doi: 10.15625/2615-9783/20366.

[13] P. N. T. Doan, H. L. Trinh, T. V. Nguyen, H. T. T. Le, and P. V. Le, “Forest fire risk prediction using geospatial data and machine learning techniques, a case study in the western region of Nghe An province,” Journal of Mining and Earth Sciences, vol. 65, no. 5, pp. 50-60, 2024, doi: 10.46326/JMES.2024.65(5).06.

[14] L. T. Thai, T. V. Tran, K. V. Le, and M. Florke Staats, “Peatmass change and water level influencing regenerated Melaleuca forest after a fire in U Minh Thuong National Park, Vietnam,” Sustainability, vol. 16, no. 2, article 620, 2024, doi: 10.3390/su16020620.
[15] T. L. Saaty, “Decision making with the analytic hierarchy process,” International Journal of Services Sciences, vol. 1, no. 1, pp. 83-98, 2008, doi: 10.1504/IJSSCI.2008.017590.
[16] J. Malczewski, “GIS-based multicriteria decision analysis: a survey of the literature,” International Journal of Geographical Information Science, vol. 20, no. 7, pp. 703-726, 2006, doi: 10.1080/13658810600661508.
[17] C. J. Tucker, “Red and photographic infrared linear combinations for monitoring vegetation,” Remote Sensing of Environment, vol. 8, no. 2, pp. 127-150, 1979, doi: 10.1016/0034-4257(79)90013-0.
[18] A. Huete, K. Didan, T. Miura, E. P. Rodriguez, X. Gao, and L. G. Ferreira, “Overview of the radiometric and biophysical performance of the MODIS vegetation indices,” Remote Sensing of Environment, vol. 83, no. 1-2, pp. 195-213, 2002, doi: 10.1016/S0034-4257(02)00096-2.
[19] B. C. Gao, “NDWI - A normalized difference water index for remote sensing of vegetation liquid water from space,” Remote Sensing of Environment, vol. 58, no. 3, pp. 257-266, 1996, doi: 10.1016/S0034-4257(96)00067-3.
[20] E. R. Hunt Jr. and B. N. Rock, “Detection of changes in leaf water content using near- and middle-infrared reflectances,” Remote Sensing of Environment, vol. 30, no. 1, pp. 43-54, 1989, doi: 10.1016/0034-4257(89)90046-1.
[21] E. Vermote, C. Justice, M. Claverie, and B. Franch, “Preliminary analysis of the performance of the Landsat 8/OLI land surface reflectance product,” Remote Sensing of Environment, vol. 185, pp. 46-56, 2016, doi: 10.1016/j.rse.2016.04.008.
[22] Z. Zhu and C. E. Woodcock, “Object-based cloud and cloud shadow detection in Landsat imagery,” Remote Sensing of Environment, vol. 118, pp. 83-94, 2012, doi: 10.1016/j.rse.2011.10.028.